RSC Advances

PAPER

View Article Online
View Journal | View Issue

Cite this: *RSC Adv.*, 2022, **12**, 23845

Green synthesis of biocompatible core–shell (Au–Ag) and hybrid (Au–ZnO and Ag–ZnO) bimetallic nanoparticles and evaluation of their potential antibacterial, antidiabetic, antiglycation and anticancer activities

Sumaira Anjum, *[a] Khadija Nawaz,[a] Bushra Ahmad,[b] Christophe Hano [c] and Bilal Haider Abbasi [d]

The fabrication of bimetallic nanoparticles (BNPs) using plant extracts is applauded since it is an environmentally and biologically safe method. In this research, *Manilkara zapota* leaf extract was utilized to bioreduce metal ions for the production of therapeutically important core–shell Au–Ag and hybrid (Au–ZnO and Ag–ZnO) BNPs. The phytochemical profiling of the leaf extract in terms of total phenolic and flavonoid content is attributed to its high free radical scavenging activity. FTIR data also supported the involvement of these phytochemicals (polyphenols, flavonoids, aromatic compounds and alkynes) in the synthesis of BNPs. Whereas, TEM and XRD showed the formation of small sized (16.57 nm) spherical shaped core–shell Au–Ag BNPs and ZnO nano-needles with spherical AuNPs (48.32 nm) and ZnO nano-rods with spherical AgNP (19.64 nm) hybrid BNPs. The biological activities of BNPs reinforced the fact that they show enhanced therapeutic efficacy as compared to their monometallic components. All BNPs showed comparable antibacterial activities as compared to standard tetracycline discs. While small sized Au–Ag BNPs were most effective in killing human hepato-cellular carcinoma cells (HepG2) in terms of lowest cell viability, highest intracellular ROS/RNS production, loss of mitochondrial membrane potential, induction of caspase-3 gene expression and enhanced caspase-3/7 activity. BNPs also effectively inhibited advanced glycation end products and carbohydrate digesting enzymes which can be used as a nano-medicine for aging and diabetes. The most important finding was the permissible biocompatibility of these BNPs towards brine shrimp larvae and human RBCs, which suggests their environmental and biological safety. This research study gives us insight into the promise of using a green route to synthesize commercially important BNPs with enhanced therapeutic efficacy as compared to conventional treatment options.

Received 20th May 2022
Accepted 16th August 2022

DOI: 10.1039/d2ra03196e

rsc.li/rsc-advances

1 Introduction

Bimetallic nanoparticles (BNPs) are more attractive from a scientific and technological viewpoint as compared to monometallic nanoparticles (NPs) due to their superior characteristics. BNPs are composed of two different metals with enhanced electronic, plasmonic, catalytic, optical, thermal, magnetic and biological properties due to a synergistic effect.[1]

The synthesis of BNPs *via* a green route is gaining particular attention as NPs are produced without any harsh synthesis conditions or using expensive and hazardous chemicals.[2] Moreover, plant mediated synthesis of BNPs has an advantage of producing biocompatible BNPs as they are capped by therapeutically important plant secondary metabolites.[3] Among different types of BNPs, gold (Au) is the most biologically prepared bimetallic nanostructure reported so far. Particularly Au–Ag nano-systems have received an enormous amount of attention. Given that, in our research we have synthesized other important BNPs including gold–zinc oxide bimetallic NPs (Au–ZnO BNPs), gold–silver bimetallic NPs (Au–Ag BNPs) and silver–zinc oxide bimetallic NPs (Ag–ZnO BNPs). These BNPs were green synthesized from *Manilkara zapota* leaf extract (LE) which is valued for its medicinal and nutritional properties. *M. zapota* is known to possess a rich content of vitamin, minerals, bioactive phenols and flavonoids,[4] therefore making it a superb

[a]*Department of Biotechnology, Kinnaird College for Women, 92-Jail Road, Lahore-54000, Pakistan. E-mail: sumaira.anjum@kinnaird.edu.pk; Tel: +92-3006957038*

[b]*Department of Biochemistry, Shaheed Benzair Bhutto Women University, Peshwar-25120, Pakistan*

[c]*Laboratoire de Biologie des Ligneux et des Grandes Cultures, INRAE USC1328, University of Orleans, 45067 Orléans Cedex 2, France*

[d]*Department of Biotechnology, Quaid-i-Azam University, Islamabad-45320, Pakistan*

candidate for the green synthesis of BNPs as these metabolites contribute in the bio-reduction, capping and stabilizing of BNPs.

Advancement in the synthesis of BNPs has paved way to their diversified applications especially in biomedicine. One of the widely explored therapeutic application of BNPs include their anti-microbial action towards Gram positive and negative multi-drug resistant microbes. The BNPs are emerging as an alternate to antibiotics which have become ineffective due to their inappropriate and inadequate use.[5] Secondly, BNPs especially Au–Ag NPs have been reported as important agents for cancer diagnosis and therapeutics as they show increased efficiency and greater stability.[6] BNPs have demonstrated a potential to treat a wide range of cancers including ovarian, lung, oral, breast and many others.[7–9] Other promising application of BNPs include their anti-diabetic and anti-aging properties.[10,11] The advantage of using green BNPs is their target specificity and biocompatibility due to phytochemical capping.[12] In this research, the therapeutic efficacy of green synthesized BNPs was evaluated including anti-bacterial activity against *Bacillus subtilis*, *Pseudomonas aeruginosa* and *Pseudomonas fluorescens*; anti-cancerous activity against HepG2 cells in terms of cell viability, intracellular ROS/RNS production, mitochondrial membrane potential and caspase-3 gene expression as well as anti-glycation, anti-diabetic and biocompatibility with brine shrimp larvae and human RBCs. According to our knowledge, this is first report in which a variety of BNPs have been synthesized from a single plant source and comparatively evaluated for their various biological activities, especially the hybrid Au–ZnO BNPs.

2 Materials and methods

2.1. *Manilkara zapota* leaves extract preparation

Leaves of *M. zapota* were plucked afresh and verified by the Department of Botany, Kinnaird College for Women, Lahore. 10 g leaves were dry weighed and washed with tap water as well as distilled water thrice. The washed leaves were set to boil in 400 mL distilled water on burner to reduce its volume up to 100 mL. The mixture was grounded with pestle and mortar and filtered with Whatman's filter paper. The filtrate LE was refrigerated at 4 °C.

2.2. Phytochemical analysis of *Manilkara zapota*

Total phenolic contents (TPC) of *M. zapota* LE were measured by Folin–Ciocalteu's method[13] while total flavonoid contents (TFC) were estimated by aluminum chloride colorimetric protocol following Khan *et al.*[13] For TPC, 1 mL LE or gallic acid standard (50–1000 μg mL^{-1}), 0.5 mL Folin–Ciocalteu's reagent and 5 mL distilled water were taken in a test-tube. The mixture was properly shaken and incubated at room temperature (RT) for 5 min, and 1.5 mL of 20% sodium carbonate and distilled water were added to make total volume 5 mL. A deep blue color of mixture developed. Lastly, the mixture was incubated for 2 h at RT and absorbance of known standard was measured at 750 nm using a spectrophotometer (Analytik Jena, Specord 200 Plus, Jena, Germany). Lastly, the TPC of LE was estimated from a gallic acid standard curve ($y = 0.00004x + 0.0089$, $R^2 = 0.9953$) and expressed as mg g^{-1} of gallic acid equivalent in milligrams per gram (mg GAE per g) of dry extract.

For TFC, 1 mL *M. zapota* extract/quercetin standard (25–200 μg mL^{-1}), 0.2 mL of 1 M potassium acetate, 5.6 mL distilled water and 0.2 mL of 10% (w/v) $AlCl_3$ were taken in a test tube, shaken and incubated for 30 min at RT. Absorbance of standard was measured at 415 nm by spectrophotometer. Lastly, the TFC of LE was determined from a quercetin standard curve ($y = 0.0057x + 0.0127$, $R^2 = 0.9973$) and expressed as quercetin equivalent (QE) per gram DW.

TPC and TFC were measured by following equation;

$$\text{TPC/TFC} = \frac{C \times V\ (\text{mL})}{m\ (\text{g})} \quad (1)$$

Free radical scavenging activity (FRSA) was evaluated to measure antioxidant potential of *M. zapota* LE using DPPH (2,2-diphenyl-1-picrylhydrazyl) according to the protocol of Anjum *et al.*[14] Briefly, 0.5 mL LE and 4.5 mL DPPH (3.2 mg/100 mL methanol) were mixed in a test tube and incubated for 1 h at RT. The absorbance of mixture and standard were measured by spectrophotometer at 517 nm. FRSA was expressed as a percentage of discoloration of DPPH calculated using the equation as follows;

$$\text{FRSA}\ (\%) = 100 \times \left(1 - \frac{\text{absorbance of plant extract}}{\text{absorbance of standard}}\right) \quad (2)$$

the experiment was run in triplicates.

2.3. Synthesis of bimetallic nanoparticles from *M. zapota*

Au–Ag BNPs were prepared using protocol as mentioned by Elemike *et al.*[15] after some changes. To synthesize Au–Ag BNPs (1 : 5), 10 mL of LE and 50 mL of 1 mM silver nitrate solution (SNS) were mixed together for 5 min followed by addition of 50 mL of 1 mM chloroauric acid. A purple color of solution developed. The solution was constantly stirred for 2 h on magnetic stirrer.

Au–ZnO BNPs (0.1/0.5) were synthesized from the method of Pandiyan *et al.*[16] 1 mL LE and 50 mL of 1 mM chloroauric acid mixture was heated for 5 min at 60 °C followed by adding 50 mL of 0.5 M zinc acetate stock solution. Whereas, Ag–ZnO BNPs (0.1/0.1) were prepared as stated by Sumbal *et al.*[17] with some changes. 1 mL LE was heated for 5 min at 60 °C with 50 mL of 0.1 M zinc acetate. After 5 min, 5 mL of 0.1 M silver nitrate for Ag–ZnO BNPs was added and pH was adjusted to 12 with dropwise addition of 2 M NaOH. The mixture was incubated at 60 °C for 2 h and stirred constantly.

The progress and synthesis of all BNPs was confirmed from UV-visible spectrophotometer. Lastly, the solutions of all BNPs were centrifuged at 10 000 rpm for 15 min, supernatant discarded and pellets were re-suspended in distilled water. This step was repeated thrice to properly wash BNPs. Finally the BNPs were dried at 40 °C overnight and subjected to characterization and biological activities.

2.4. Characterization of BNPs

BNPs were characterized for their physico-chemical properties from various techniques including UV-visible spectroscopy, Transmission Electron Microscopy (TEM), X-ray Diffraction (XRD), Fourier-Transform Infrared Spectroscopy (FTIR) and Dynamic Light Scattering (DLS).

Green synthesis of BNPs was monitored by recording their UV-vis spectra by spectrophotometer. FTIR analysis was carried out as stated by Tungmunnithum *et al.*[18] using Brucker (Palaiseau, France) V70 interferometer. The wave numbers were measured in the range 400–4500 cm^{-1}.

The shape of BNPs was evaluated from TEM (JEM-2100, JEOL Ltd., Tokyo, Japan) by dissolving 1 mg BNPs in 1 mL of 50% ethanol and sonicated for 25 min to ensure proper mixing. 10 μL BNPs were dropped onto a para-film and a grid was placed over it for 5–10 min. The following day BNPs were observed under TEM.[19]

The crystallinity of BNPs was evaluated by XRD using an X-ray diffractometer (Shimadzu-Model, XRD6000). Furthermore, the size of BNPs was determined by the Debye–Scherrer equation.[20]

DLS was applied to measure the size distribution of BNPs with the help of Zetasizer (Malvern, NanoZSP, UK) as reported by Sohail *et al.*[21]

2.5. Antibacterial activity of BNPs

The potential of BNPs as antibacterial agents was assessed against *Bacillus subtilis*, *Pseudomonas aeruginosa* and *Pseudomonas fluorescens* by well-diffusion method as described by Abbasi *et al.*[22] The stock cultures of *B. subtilis*, *P. aeruginosa* and *P. fluorescens* were revived on nutrient agar followed by swabbing a single colony of bacterial strains on Mueller Hinton Agar (MHA). 15 μL of LE as a negative control while positive controls 1 mM chloroauric acid–silver nitrate solution (CAA–SNS), 0.1 M chloroauric acid solution–0.5 M zinc acetate (CAA–ZAS) and 0.1 M silver nitrate–zinc acetate solution (SN–ZAS) were added. 15 μL 10 mg mL^{-1} BNPs and 10 μg per disc tetracyclin antibiotic discs (Thermo Fisher Scientific™ Oxoid™) were added to the wells on MHA plates. The plates were incubated at 37 °C overnight and the zones of inhibition in millimeter (mm) were measured.

2.6. Biocompatibility of BNPs

2.6.1. Lethality of BNPs against brine shrimp. Lethality of BNPs was measured against *Artemia salina* (brine shrimp) in a 96-well plate for 24 h as stated by Ahmed *et al.*[23] Firstly *A. salina* eggs were hatched by incubating eggs for 24–48 h in a plastic tray containing 38 g L^{-1} sterile sea water supplemented with dried yeast (6 mg L^{-1}) and proper oxygen supply. Ten mature nauplii (phototropic) were taken and BNPs (25–200 μg mL^{-1}) were added to the well and final volume was made up to 300 μL. 1% DMSO in sea water was used as a negative control whereas doxorubicin as a positive control. Lethal concentration (LC_{50}) was measured by using table curve 2D v5.01 of BNPs with ≥50% mortality.

2.6.2. Biocompatibility of BNPs with human red blood cells (hRBCs). Hemo-compatibility of BNPs with RBCs was measured by using blood samples of healthy six female and six males (about 28–35 years old) after obtaining their written consent. Procedures dealing with human subjects were carried out in consideration with the ethical standards of International and National Research Committees and with the 1964 Helsinki Declaration and its later amendments. Blood samples were collected in EDTA vacutainers which prevents blood clotting. This experiment was performed in consideration with the ethical standards of the International and National Research Committees as well as 1964 Helsinki Declaration and its later amendments due to the involvement of human participants.[24] After extracting RBCs, erythrocytes and 100 μL BNPs were taken in an Eppendorf Tube which were incubated at 35 °C for 1 h and centrifuged at 10 000 rpm for 10 min. 100 μL supernatant was taken in a 96-well plate and BioTek ELX800 Absorbance Microplate Reader (BioTek Instruments, France) was used to measure the release of hemoglobin at 540 nm. Triton X-100 (positive) and DMSO (negative) acted as controls. The results were expressed as % hemolysis measured by the below stated formula:[24]

$$\text{Hemolysis } (\%) = \frac{\text{sample absorbance} - \text{negative control absorbance}}{\text{positive control absorbance} - \text{negative control absorbance}} \times 100 \quad (3)$$

2.7. Anti-diabetic and anti-glycation activities of BNPs

Anti-diabetic activity of BNPs was determined in terms of inhibition of α-glucosidase and α-amylase as reported by Hano *et al.*[25] α-Amylase inhibition by BNPs was evaluated by using porcine pancreatic α-amylase (Sigma Aldrich). For α-glucosidase inhibition assay, 1 μL rat intestinal fluid having 4-nitrophenyl-α-D-glucopyranoside (5 mM, 4NPG; Sigma, France) was used by a chromogenic method as described in (ref. 26). The antidiabetic activity was reported as % inhibition of both enzymes.

The anti-glycation activity of BNPs was measured as % inhibition of AGEs as mentioned by Shah *et al.*[26] BNPs were mixed with 20 mg mL^{-1} bovine serum albumin (Sigma Aldrich) prepared in phosphate buffer (0.1 M; pH 7.4), 1 mL of phosphate buffer containing sodium azide 0.02% (w/v) and glucose solution (0.5 M; Sigma Aldrich) were incubated for 5 days at 37 °C in dark. The formation of fluorescent AGEs monitored by VersaFluor fluorometer (Bio-Rad, France) set at 410 nm emission and 330 nm excitation wavelengths and % inhibition was calculated.

2.8. Anti-cancerous activities of BNPs

2.8.1. Measurement of cell viability of HepG2 cells. Cell viability of human liver cancer cells (HepG2) (ATCC HB-8065; American Type Culture Collection, USA) was measured by using 3-(4,5-dimethylthiazolyl-2)-2,5-diphenyltetrazolium bromide (MTT) dye. HepG2 cells were cultured in Dulbecco's Modified Eagle Medium. 200 μg mL^{-1} BNPs were added in a 96-well plate, pre-seeded with HepG2 cells (>90% viability; 200 μL per well; 1×10^4 cells per well), for 24 h 10 μL MTT dye (5 mg mL^{-1}) was added and incubated for 3 h. Insoluble formazan formed was dissolved with 10% acidified sodium dodecyl sulfate. Cells incubated overnight were put to microplate reader (Platos R, 496. AMP, AMEDA Labordiagnostik GmbH, Graz, Austria) to measure their absorbance at 570 nm. Non-treated cells (NTC) were used as a control. Cell viability was expressed as percentage and measured from the below mentioned equation:[27]

$$\text{Viability } (\%) = \frac{\text{sample absorbance} - \text{control absorbance}}{\text{NTC absorbance} - \text{media absorbance}} \times 100 \quad (4)$$

2.8.2. Evaluation of intracellular reactive oxygen and nitrogen species (ROS/RNS) production. Production of intracellular ROS/RNS was measured by following the method of Nazir *et al.*[28] In a 96-well plate, pre-seeded HepG2 cells were washed with phosphate-buffer saline (PBS) twice and suspended in PBS having 0.4 μM fluorescent dihydrorhodamine-123. The mixture was incubated in dark for 10 min at 30 °C and its fluorescence measured ($\lambda_{em} = 535$ nm, $\lambda_{ex} = 505$ nm) with a VersaFluor fluorometer (Bio-Rad, France).

2.8.3. Mitochondrial membrane potential (MMP) measurement. BNPs resulted in a loss of MMP which was measured by following protocol of Khan *et al.*[13] HepG2 cells were incubated in a culture media containing 25 nM using 3,3′-dihexyloxacarbocyanine iodide for 40 min at 37 °C. Mitochondrial membrane potential was reported as relative fluorescent units (RFU).

2.8.4. Caspase-3 gene expression and caspase-3/7 activity. To measure the expression of caspase-3 gene, firstly isolation of total RNA was carried out from GeneJET RNA Purification Kit (Thermo Scientific) followed by quantification of using Quant-iT RNA Assay Kit (Invitrogen). The reverse transcription of RNA was carried out by using first-strand cDNA synthesis kit (Thermo). PikoReal quantitative PCR was performed using DyNAmoColor-Flash SYBR Green qPCR Kit (Thermo Fisher). Caspase-3 primers were: 5′-CACGCCATGTCATCATCAAC-3′ (reverse primer) and 5′-TGTTTGTGTGCTTCTGAGCC-3′ (forward primer) (PCR product size: 210 bp). Data was analyzed by Pikoreal software.

Apo-ONE Homogeneous Caspase-3/7 Assay kit (Promega) helped to evaluate *in vitro* caspase-3/7 activity by following manufacturer's instructions. All the data was measured in triplicates.

2.9. Data analysis

Mean and standard deviation (SD) of all data was calculated with the help of SPSS (Windows Version 7.5.1, SPSS Inc., Chicago, IL, USA). The data was expressed as mean ± SD.

3 Results and discussion

3.1. Phytochemical analysis of *Manilkara zapota*

Phenolic compounds form an important constituent of plants as they bear a hydroxyl group which impart them the free radical scavenging potential.[29] Whereas flavonoids are a subgroup of polyphenols which have important pharmacological role as free radical scavengers.[30] Recently, metabolic profiling of *M. zapota* leaves detected the presence of secondary metabolites including flavonoids and phenolic compounds.[31] The phytochemical analysis of *M. zapota* LE was carried out in this study which revealed TPC and TFC to be 67.16 ± 2.31 mg GAE per g DW and 18.27 ± 0.95 mg QE per g DW respectively. Previous study also shows enriched phenolic and flavonoid content present in aqueous LE of *M. zapota* reporting TPC 106.19 ± 1.99 mg GAE per g and TFC to be 37.04 ± 0.37 mg QE per g.[32] Since the ability of plant extract to fabricate stable NPs depends on their phytochemical profile, here the enriched flavonoid and phenolic content present in *M. zapota* LE show their potential to effectively synthesize BNPs.[33]

A single assay cannot be the representative of the antioxidant potential of plant extract. Therefore we have also performed the DPPH assay in which when DPPH is mixed with the test substance, reduced form of DPPH *i.e.* diphenypicrylhydrazine forms with a loss of violet color.[34] The FRSA of *M. zapota* LE was 80.04 ± 1.28%, which correlates with the flavonoid and phenolic contents present in the LE. Kaneria and Chanda also reported good FRSA (65.41%) of aqueous extract of *M. zapota* which was comparable to other solvent extracts.[32] The plant extract exhibits strong antioxidant activity attributed to its phytochemical profile which means it can chelate metal ions and reduce it into BNPs effectively.

3.2. Characterization of BNPs

3.2.1. UV-visible spectroscopy. Visual color change of reaction mixture is a first indication of NPs formation. Similarly colorless to greyish blue change of color indicated the synthesis of Au–ZnO. Furthermore, UV-visible spectroscopy helped to evaluate the progress of BNPs synthesis as well as characterize them from distinct peaks. Fig. 1A shows a major peak at 570 nm for AuNPs while a shoulder peak at 355 nm for ZnONPs. Similar UV-visible spectrum was observed by Khan *et al.*[35] where a peak at 537 nm and a shoulder peak at 351 nm was observed for biogenic Au–ZnO core shell NPs.

Visually brown to deep purple color development indicated the synthesis of Au–Ag BNPs. Weng *et al.*[36] also reported purple color formation of the mixture of Au–Ag BNPs during synthesis by using *Deinococcus radiodurans* protein extract. UV-visible spectroscopic analysis of Au–Ag BNPs was recorded as shown in Fig. 1B. Wavelength at 530 nm was observed which is in agreement with previous results for 1 : 1 Au–Ag BNPs where single sharp peak centered at 559 nm was observed.[37] Moreover, single peak indicates that Au–Ag BNPs are in an alloy form and not a heterogeneous mixture of individual NPs. Likewise, soybean leaf extract-mediated Au–Ag BNPs also showed a single peak at 533 nm.[38]

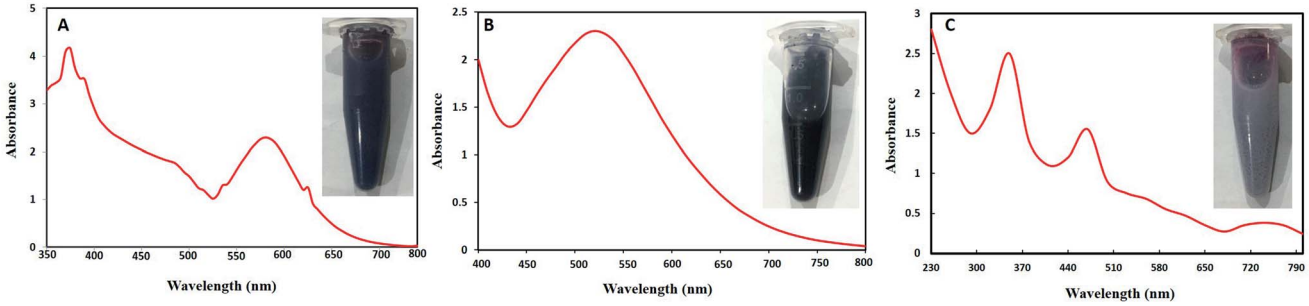

Fig. 1 UV-visible profile of (A) Au–ZnO BNPS (B) Au–Ag BNPs (C) Ag–ZnO BNPs.

Fig. 1C shows a dark brown color of reaction mixture of Ag–ZnO BNPs as well as absorption peaks at 350 nm for ZnONPs and at 470 nm for AgNPs. Sumbal *et al.*[17] also reported brown colored mixture of ZnO–AgNPs when prepared at ratio 0.5 : 0.5 (v/v). These peaks are characteristic of pure zero valent ZnO and AgNPs confirming that prepared BNPs are composed of Ag–ZnO. Previously, peaks at 355 nm and 450 nm were observed for bimetallic ZnO–AgNPs from UV-visible spectroscopy.[39] Moreover, two characteristic SPR band between 400–480 nm and 350 and 380 nm were reported for bimetallic Ag–ZnONPs by Anjum *et al.*[40] when synthesized from *Morus macroura* leaf extract.

3.2.2. FTIR analysis. FTIR is a widely used technique for chemical characterization of NPs at molecular level.[41] FTIR analysis of plant extract and BNPs shows a complex nature of phytochemicals present in the extract which have bio-reduced and capped the synthesized BNPs. Fig. 2A shows FTIR spectra for *M. zapota* LE showing major and minor peaks at 621 cm^{-1}, 1068 cm^{-1}, 1332 cm^{-1}, 1433 cm^{-1}, 1647 cm^{-1}, 1971 cm^{-1}, 2094 cm^{-1}, 2443 cm^{-1} and 3356 cm^{-1}. In Fig. 2B Au–ZnO BNPs displayed absorbance peaks at ~599 cm^{-1}, 1043 cm^{-1}, 1309 cm^{-1}, 2150 cm^{-1}, 2411 cm^{-1} and 3319 cm^{-1}. Whereas Fig. 2C also shows similar absorbance peaks for Au–Ag BNPs at ~603 cm^{-1}, 1018 cm^{-1}, 1305 cm^{-1}, 2148 cm^{-1}, 2409 cm^{-1}, 3219 cm^{-1} and 3649 cm^{-1}. Lastly, absorption peaks at ~603 cm^{-1}, 1016 cm^{-1}, 1652 cm^{-1}, 2189 cm^{-1}, 3408 cm^{-1} and 3543 cm^{-1} were recorded for Ag–ZnO BNPs as shown in Fig. 2D. According to literature the absorption peaks between 3649–3219 cm^{-1} are representative of free hydroxyl and H-bonded stretch of alcohols and phenols.[42] Peaks between 2094–2443 cm^{-1} corresponds to the weak stretching of C≡C

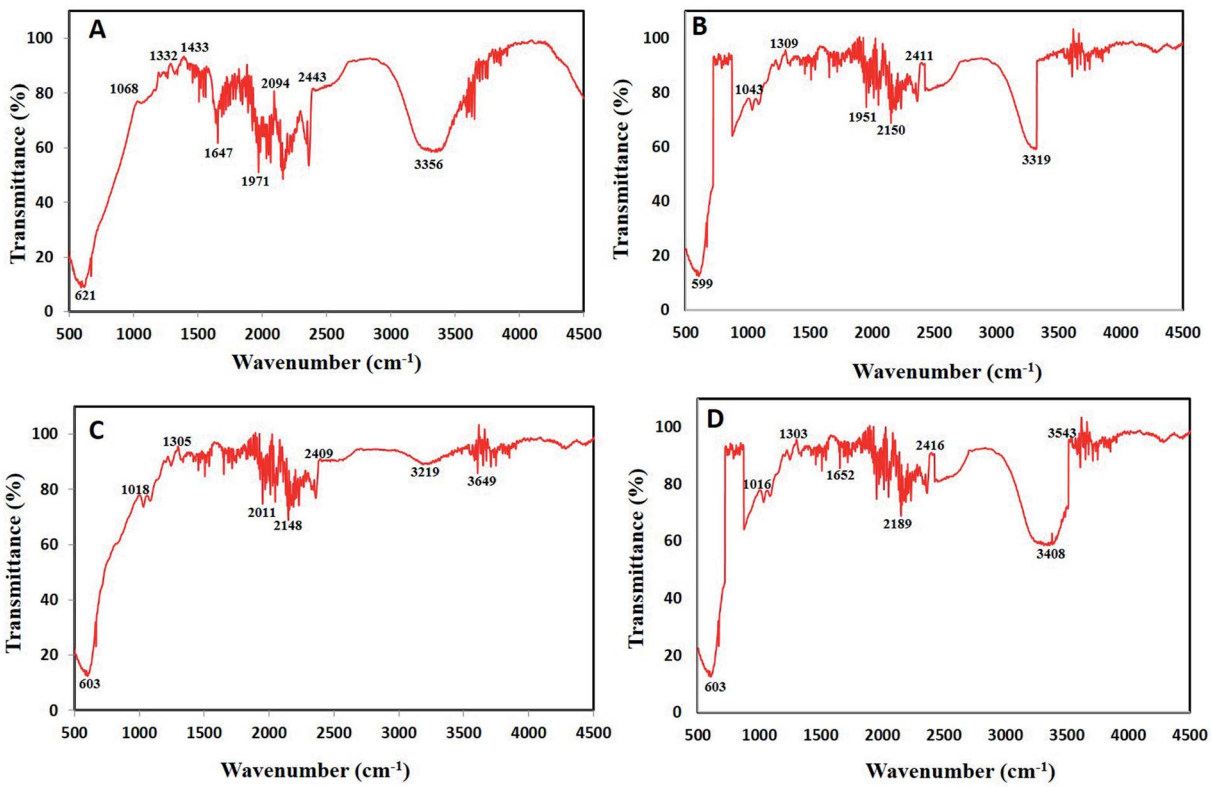

Fig. 2 FTIR data of (A) *Manilkara zapota* LE (B) Au–ZnO BNPS (C) Au–Ag BNPs (D) Ag–ZnO BNPs.

stretching of alkynes.[43] Wavenumber at 599–621 cm^{-1} represents =C–H bend of alkenes.[44] Lastly, strong peaks between 1068–1305 cm^{-1} represents C–O stretch of carboxylic acids and alcohols while wavenumbers 1647–1652 cm^{-1} represents C–C stretch of aromatic compounds.[45,46]

The present data recommends the involvement of various phytochemicals such as polyphenols, flavonoids, aromatic compounds, carboxylic acid, alkenes and alkynes in the process of bioreduction as well as capping of BNPs. Similarly, Kuppusamy *et al.*[47] also demonstrated *via* FTIR analysis that functional groups like amine, alkane, phenol and alcohol present in *Commelina nudiflora* plant extract played vital role in Au–Ag NPs alloy synthesis. These antioxidant phytochemicals play role during synthesis by donating hydrogen atom/electrons to reduce the metal salt into zero valent state which nucleate to form NPs.[48] Lastly, phytochemicals act as stabilizing agents which cap the NPs. These bio-stabilized NPs are more biocompatible having better biological activities.[49]

3.2.3. TEM analysis. TEM images gave us an insight into the shapes of BNPs. Fig. 3A and B depicts transmission electron micrographs of hybrid Au–ZnO BNPs, upon careful observation the needle shaped ZnONPs are surrounded by spherical shaped AuNPs. Since green synthesis of Au–ZnO BNPs is not widely researched, various studies including physical, chemical or biological route of synthesis have mostly reported core–shell type bimetallic Au/ZnO NPs.[50,51] Our Au–ZnO BNPs resembles with the hybrid gold-doped ZnO nano-needles which were formed from *Pennisetum purpureum* leaf extract.[52] TEM images of Au–Ag BNPs suggest spherical shaped core–shell type of these NPs (Fig. 3C and D). Csapó *et al.*[53] reported similar shaped Au–

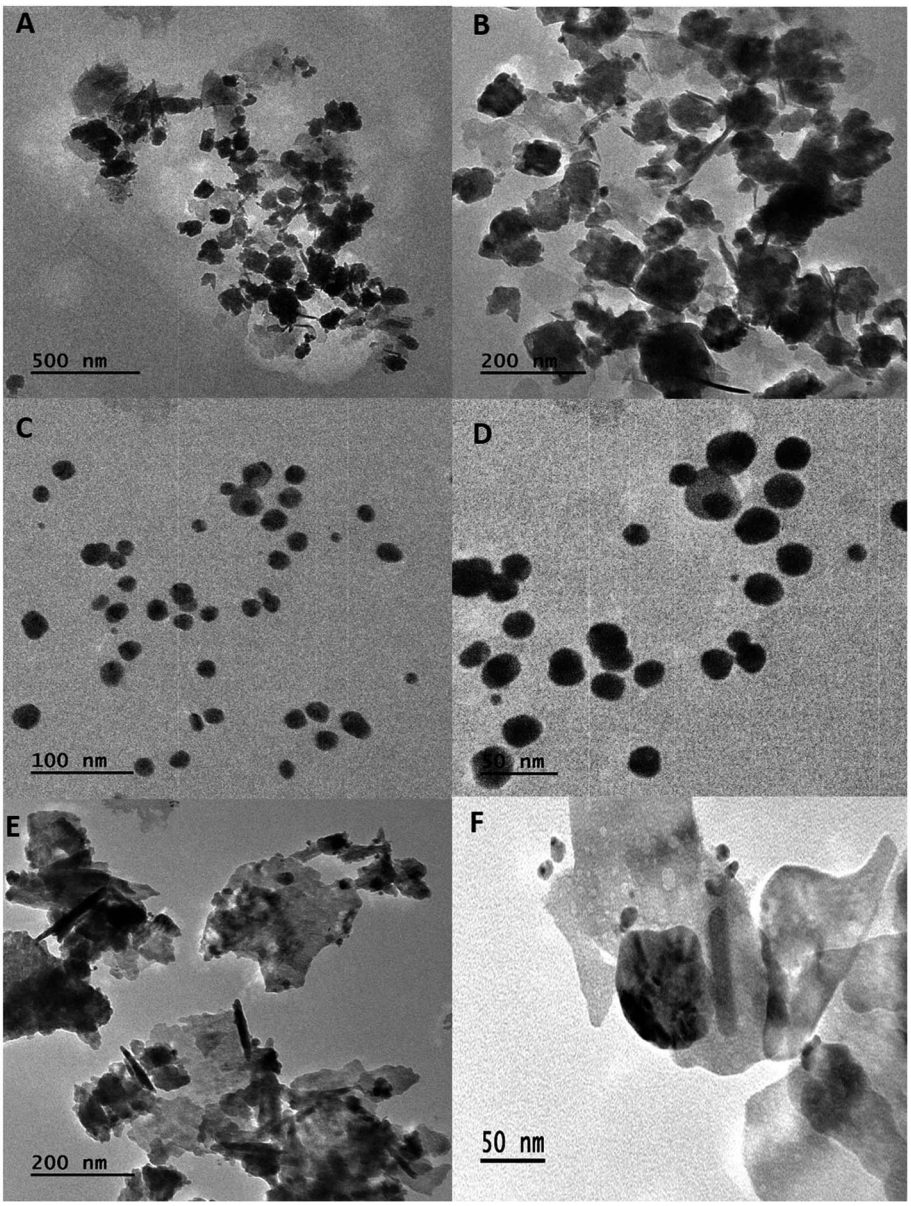

Fig. 3 Transmission electron micrographs (A and B) Au–ZnO BNPS (C and D) Au–Ag BNPs (E and F) Ag–ZnO BNPs.

Ag BNPs alloy from TEM analysis which were synthesized *via* chemical method. Ganaie *et al.*[54] also reported similar micrographs of Au–Ag core shell BNPs which were synthesized from *A. leptopus* extract. Fig. 3E and F confirms the formation of hybrid Ag–ZnO BNPs in which nano-rods ZnO are surrounded by spherical shaped AgNPs. Sali *et al.*[55] also observed deposition of spherical AgNPs onto ZnO nanorods. Slathia *et al.*[56] observed similar morphology of Ag–ZnO nanocomposites using scanning electron microscopy in which spherical AgNPs were deposited on rod shaped ZnONPs. Since different precursor salts in different types are BNPs are used, they interacted differently with each other, hence forming a variety of shapes. Here it is also observed that the rod or needle like shape of ZnO and spherical shapes of Au and Ag are consistent despite the difference in the type of metal it is paired with as a BNPs.

3.2.4. XRD analysis. XRD diffractogram of hybrid Au–ZnO BNPs is depicted in Fig. 4A which reveals about their crystallinity, purity and phase. Major reflection peaks observed at 2θ were 31.65°, 34.4°, 36.2°, 47.75°, 56.65°, 62.7°, 67.85° and 69.3° which are related to 100, 002, 101, 102, 110, 103, 112 and 201 crystal planes of hexagonal wurtzite, respectively. Absence of any characteristic impurity peaks indicates high quality of Au–ZnO BNPs. Fageria *et al.*[57] reported hexagonal crystalline structure of Au–ZnO BNPs with similar XRD pattern. Similar peaks were observed for Au–ZnO nanoflowers.[58] Furthermore, size of Au–ZnO BNPs was calculated from XRD data which was found to be 48.32 nm. Cumin seed extract synthesized bimetallic Au–ZnONPs showed face centered cubic (FCC) crystalline structure on hexagonal ZnO in a size range of 10–15 nm.[59] This shows variety of size and crystalline structure of BNPs can be synthesized by varying the plant extracts.

XRD pattern of core–shell Au–Ag BNPs showed FCC structure as peaks at 2θ were 38.3°, 44.25°, 64.05° and 77.75° which corresponds to the 111, 200, 220 and 311 planes, respectively (Fig. 4B). Additionally the reflections in XRD diffractogram resembles to the monometallic Au and Ag NPs without any peak of impurity. The crystalline structure of Au–Ag BNPs is analogous to the one stated by Kumari *et al.*[60] when BNPs were green synthesized from pomegranate juice. Similar crystalline structure of bimetallic Au–AgNPs was reported previously from XRD data.[61] The LE of *M. zapota* promoted the formation of smaller sized Au–Ag BNPs 16.57 nm as calculated by Debye Scherrer formula using XRD data. Biogenic synthesis of Ag–Au BNPs from a polymer kondagogu resulted in the formation of 21.6 nm sized NPs.[62]

The crystalline structure of hybrid Ag–ZnO BNPs was examined from XRD pattern as shown in Fig. 4C in which major and minor peaks observed at 2θ were 31.8°, 34.3°, 36.1°, 38.2°, 47.65°, 56.7°, 62.7° and 67.85°. These peaks correspond to the reflection planes 100, 002, 101, 111, 102, 110, 103 and 112 of hexagonal (ZnO) and FCC (Ag) structure nature, respectively. Moreover the average diameter of Ag–ZnO BNPs was 19.64 nm while the identified peaks indicate the purity of BNPs. Zare *et al.*[63] showed the formation of very small 5 nm sized Ag–ZnO nanocomposites having similar crystallinity synthesized by using *T. vulgaris* extract. Moreover, minor peaks for Ag while major peaks for ZnO were observed in XRD pattern for plate and spherical shaped bimetallic Ag–ZnO NPs prepared from *Silybum marianum*.[64]

3.2.5. DLS analysis. DLS provides a measure of size distribution of NPs from the scattered light in a solution.[65] Fig. 5A–C reports the size distribution of BNPs measured by DLS. Size distribution of Au–ZnO BNPs was between 20–100 nm, Au–Ag BNPs 1–60 nm and Ag–ZnO BNPs 10–70 nm. This data is in coherence with the size calculated from XRD data as highest intensity of size distribution was recorded at 50 nm (Au–ZnO BNPs) and 20 nm (Au–Ag BNPs and Ag–ZnO BNPs). Khan *et al.*[66] showed average size of Au/ZnO nanocomposites synthesized from *Hibiscus Sabdariffa* extract to be 134.3 nm measured from DLS technique. The average size of Au–Ag bimetallic NPs fabricated from *E. coli* was also measured from DLS to be 23.01 nm.[67] The diameter of *Trigonella foenum-graecum* mediated Ag–ZnO nanocomposites was between 60–90 nm as measured from DLS having similar spherical-rod shaped morphology as our Ag–ZnO BNPs.[68] Here DLS gives us an insight into the size distribution of BNPs which corresponds with the size calculated by XRD data.

3.3. Biological activities of bimetallic NPs

3.3.1. Antibacterial activity. Bimetallic NPs can serve as antibacterial agents and complement the role of antibiotics in treating bacterial infections. BNPs mediate their antibacterial action by disrupting the bacterial membrane, inducing oxidative stress and causing damage to proteins and bacterial DNA.[69] We have also explored the potential of green synthesized BNPs as antibacterial agents against *B. subtilis*, *P. aeruginosa* and *P.*

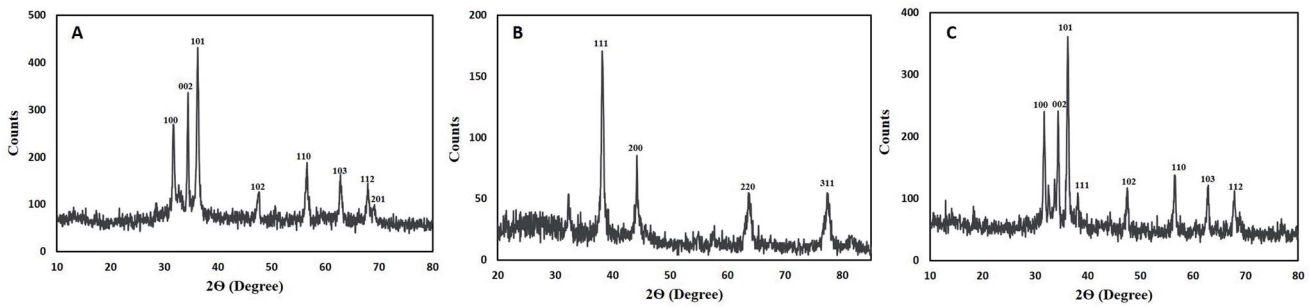

Fig. 4 X-ray diffractogram (A) Au–ZnO BNPS (B) Au–Ag BNPs (C) Ag–ZnO BNPs.

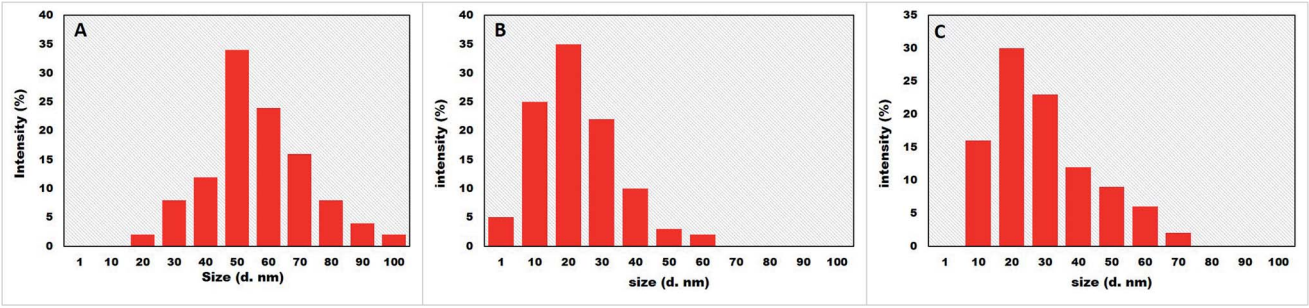

Fig. 5 DLS data (A) Au–ZnO BNPS (B) Au–Ag BNPs (C) Ag–ZnO BNPs.

fluorescens by well diffusion method (Table 1). Fig. 6A–C represents the antibacterial activities of BNPs against *B. subtilis* where Au–ZnO as well as Ag–ZnO BNPs inhibited the bacterial growth forming 12 mm zone of inhibition while Au–Ag BNPs formed 11.5 mm. This shows the significant antibacterial activity of BNPs which is comparable to that of standard antibiotic tetracycline discs. Bankura *et al.*[70] studied the antibacterial efficacy of Au–Ag alloy which was synthesized by dextran. The BNPs showed significant activity against *P. aeruginosa*, *B. cereus* and *B. subtilis* forming zone of inhibition 20, 21 and 24 mm.

Antibacterial activity of BNPs against *P. aeruginosa* were shown in Fig. 6D–F. The zone of inhibitions were measured to be Au–ZnO BNPs 15.5 mm, Ag–ZnO BNPs 12.5 mm and Au–Ag BNPs 8.5 mm. Their antibacterial activity is better than tetracycline disc which formed zone of inhibition 8–9 mm. Whereas Fig. 6G–I shows that Au–ZnO BNPs formed the highest zone of inhibition 11 mm, Ag–ZnO BNPs 9.5 mm and least by Au– Ag BNPs 8.5 mm against *P. flourescens*. Tetracycline discs formed inhibition zone of around 8–9 mm. Bimetallic Ag–ZnO nanostructure, having star-shaped ZnONPs and spherical, rod and plate shaped AgNPs showed better antibacterial activity against *P. aeruginosa* in comparison with pure ZnONPs.[71]

Here it is observed that in all bacterial strains, Gram positive or negative, the ZnO nano-rods combined with spherical AuNPs and AgNPs have shown superior antibacterial activity as compared to spherical Au–Ag BNPs. This suggest morphology based antibacterial activity of BNPs due to higher penetrative ability and surface area of nano-rods as compared to nanospheres. This further reinforces the fact that catalytic, optical, magnetic and biological activities of BNPs are improved to a greater extent in comparison to monometallic NPs.[3] Similar observation was made by Alshareef *et al.*[72] that truncated octahedral Ag–Au BNPs were more effective in killing *Enterococcus faecium* and *Escherichia coli* in comparison with spherical AgNPs.

3.3.2. Biocompatibility studies of BNPs. Brine shrimp lethality assay is performed to monitor the lethality of heavy metal, metal ions, nanoparticles and plant bioactive compounds. This assay is a routine in applied toxicology and research because of its simplicity, low-cost and small sample size requirement.[73] We have also demonstrated the biocompatibility of green synthesized bimetallic NPs through brine shrimp lethality assay in order to ensure their environmental and aquatic safety. Fig. 7A depicts LC_{50} values of Ag–ZnO BNPs (21.63 ± 0.61 μg mL^{-1}), Au–Ag BNPs (25.73 ± 2.5 μg mL^{-1}) and

Table 1 Zone of inhibition measured in mm against *B. subtilis*, *P. aeruginosa* and *P. flourescens* bacterial strains[a]

Strain type	Sample type	Zone of inhibition (mm) (15 μL per well) Ag–Au BNPs	Sample type	Zone of inhibition (mm) (15 μL per well) Au–ZnO BNPs	Sample type	Zone of inhibition (mm) (15 μL per well) Ag–ZnO BNPs
Bacillus subtilis	LE	5 ± 0.24	LE	6 ± 0.28	LE	5 ± 0.24
	CAA–SNS	11 ± 0.86	CAA–ZAS	16 ± 1.46	SN–ZAS	10 ± 0.78
	Ag–Au BNPs	11.5 ± 1.02	Au–ZnO BNPs	12 ± 1.26	Ag–ZnO BNPs	12 ± 0.79
	Antibiotic disc	15 ± 1.46	Antibiotic disc	13 ± 1.01	Antibiotic disc	12.5 ± 1.21
Pseudomonas aeruginosa	LE	5 ± 0.24	LE	5 ± 0.24	LE	5 ± 0.24
	CAA–SNS	6.5 ± 0.30	CAA–ZAS	13.5 ± 1.21	SN–ZAS	9.5 ± 0.40
	Ag–Au BNPs	7.5 ± 0.42	Au–ZnO BNPs	15.5 ± 1.36	Ag–ZnO BNPs	12.5 ± 1.32
	Antibiotic disc	8 ± 0.41	Antibiotic disc	7.5 ± 0.36	Antibiotic disc	11 ± 1.12
Pseudomonas flourescens	LE	5 ± 0.24	LE	5 ± 0.24	LE	5 ± 0.24
	CAA–SNS	9.5 ± 0.44	CAA–ZAS	8.5 ± 0.46	SN–ZAS	8.5 ± 0.40
	Ag–Au BNPs	8.5 ± 0.36	Au–ZnO BNPs	11 ± 0.42	Ag–ZnO BNPs	9.5 ± 1.12
	Antibiotic disc	8 ± 0.38	Antibiotic disc	8.5 ± 0.41	Antibiotic disc	9 ± 0.48

[a] LE represent to leaf extract, CAA–SNS to chloroauric acid–silver nitrate solution, CAA–ZAS to chloroauric acid–zinc acetate solution and SN–ZAS to silver nitrate–zinc acetate solution.

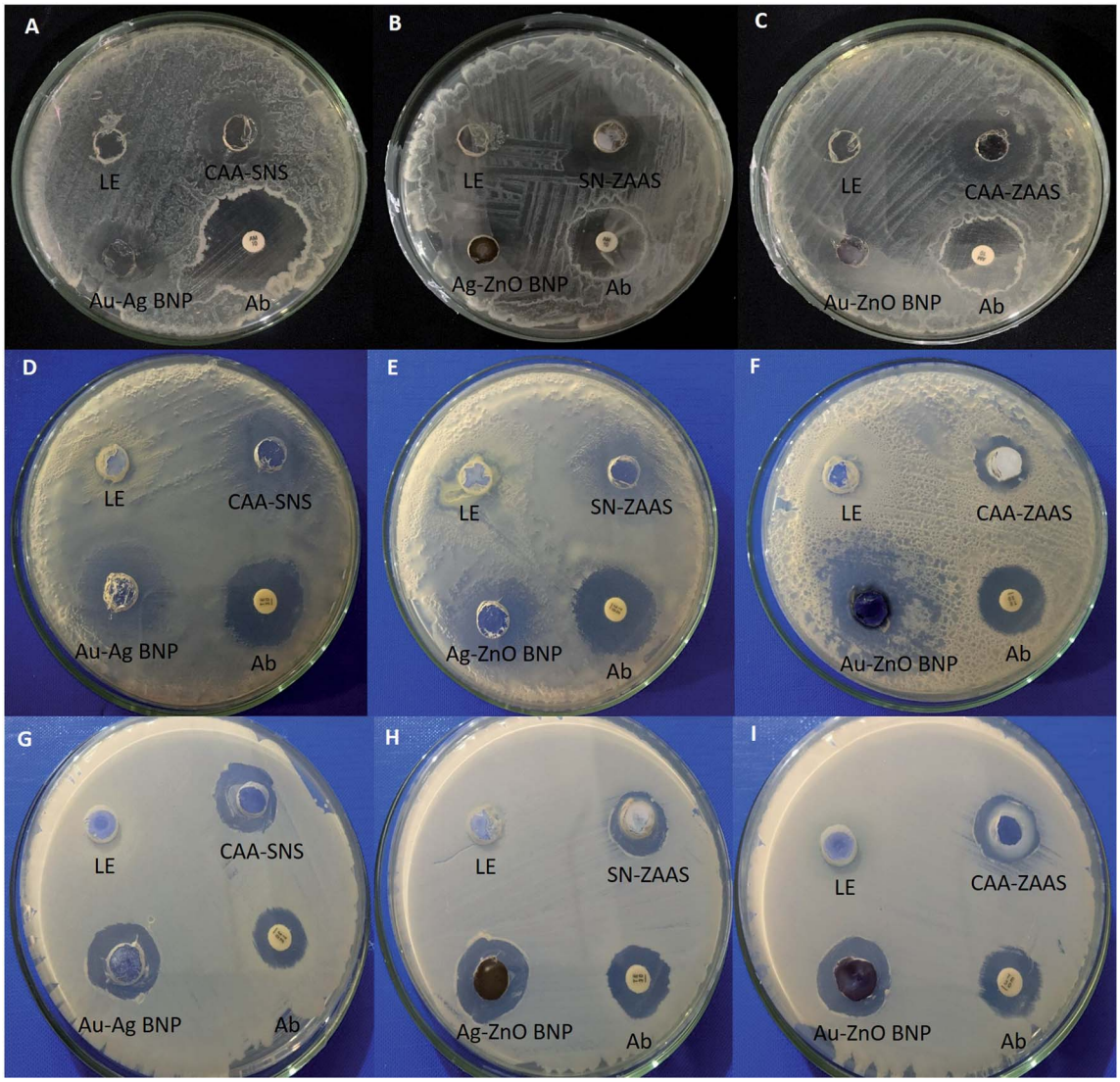

Fig. 6 Antibacterial activity of bimetallic NPs.[5] (A–C); *B. subtilis* (D–F); *P. aeruginosa* (G–I) *P. flourescens*. Note: LE represent to leaf extract, Ab to tetracycline antibiotic disc, CAA–SNS to chloroauric acid–silver nitrate solution, CAA–ZAS to chloroauric acid–zinc acetate solution and SN–ZAS to silver nitrate–zinc acetate solution.

Au–ZnO BNPs (20.96 ± 1.89 μg mL^{-1}). The results show moderately toxic nature of BNPs towards brine shrimps as LC_{50} between 1–10 μg mL^{-1} represents toxic compounds; LC_{50} 10–30 μg mL^{-1} moderately toxic compounds; LC_{50} 30–100 μg mL^{-1} mildly toxic compounds and >100 μg mL^{-1} for non-toxic.[27] Moreover, doxorubicin was used as a control which was found to be highly toxic (LC_{50} 5.92 μg mL^{-1}). *Artocarpus heterophyllus* extract prepared Ag–Au NPs showed LC_{50} value < 1000 μg mL^{-1} making them non-toxic.[74] Previously Anjum *et al.*[40] also demonstrated moderately toxic nature of *Morus macroura* mediated Ag–ZnO BNPs as well as their monometallic counterparts towards brine shrimps. These findings show a hidden efficacy of green synthesized bimetallic NPs for applications like antioxidant, anti-cancerous and antimicrobial.

Biocompatibility with human RBCs was also assessed to evaluate their % hemolysis as shown in Fig. 7B. All bimetallic NPs were found only slightly hemolytic as Ag–ZnO BNPs were 3.16 ± 0.18%, Au–Ag BNPs 4.22 ± 0.34 and 3.76 ± 0.53% hemolytic. Magnetite/silver NPs showed negligible hemolysis 1% at concentration up to 200 μg mL^{-1} while increase in hemolysis was observed with increase in concentration.[75] Another type of Ag–Pd NPs were also found biocompatible with RBCs up to its maximum dose of 200 μg mL^{-1}.[76] Our BNPs are also safe for human use as an alternate drug since 5% hemolysis is acceptable for biomaterials.[77]

3.3.3. Anti-diabetic and anti-glycation activities of BNPs. Hyperglycemia can be regulated by inhibiting carbohydrate catalyzing enzymes such as α-glucosidase and α-amylase thereby preventing the catalysis of complex sugars into monosaccharides.[78] In this regard, NPs have significant therapeutic potential in controlling diabetes by inhibiting carbohydrate hydrolyzing enzymes. The anti-diabetic activity of BNPs was determined as % inhibition of α-glucosidase and α-amylase as represented in Fig. 8A. Ag–ZnO BNPs led to the highest inhibition

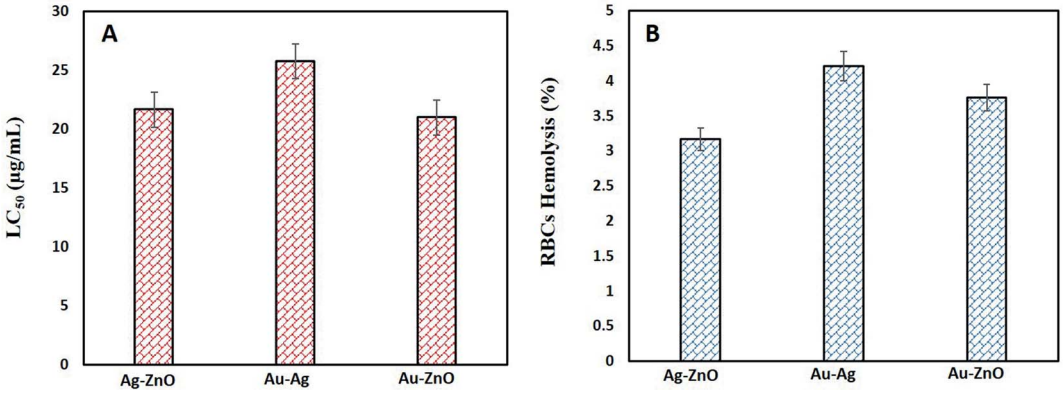

Fig. 7 Biocompatibility studies (A) toxicity of BNPs against brine shrimp larvae (B) % hemolysis of human RBCs by BNPs.

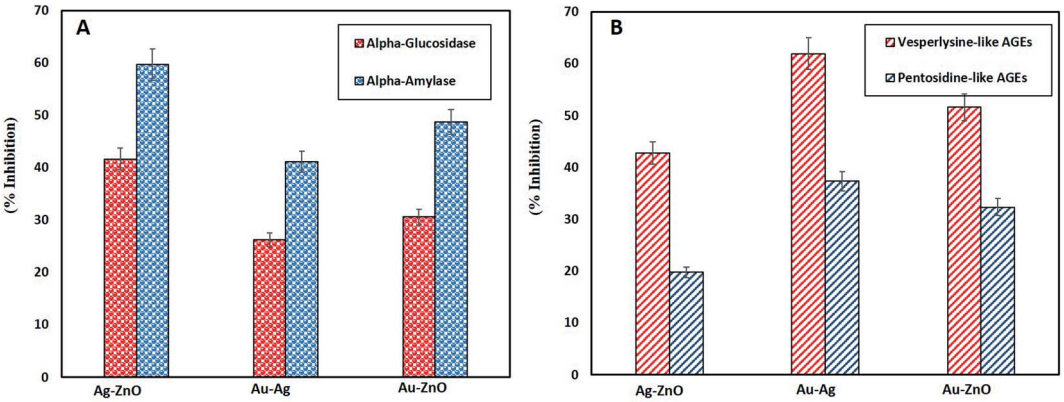

Fig. 8 (A) Anti-diabetic activity of BNPs (B) anti-glycation activity of BNPs.

of α-glucosidase (41.6 ± 1.00%) and α-amylase (59.7 ± 1.01%), followed by Au–ZnO BNPs 30.6 ± 0.26% and 48.73 ± 0.70%, respectively. Au–Ag BNPs resulted in 26.24 ± 1.01% and 41.13 ± 0.67% inhibition of α-amylase and α-glucosidase, respectively. Green Au–Ag BNPs produced from the *Ocimum basilicum* extract resulted in inhibition of α-amylase 69.97 ± 3.42% inhibition and 85.77 ± 5.82% α-glucosidase enzyme.[79] Here, ZnO nano-needles and nano-rods combined with Au and Ag enhanced the efficacy of BNPs in inhibiting carbohydrates hydrolyzing enzymes as compared to core–shell Au–Ag BNPs. Similarly, Robkhob *et al.*[80] also demonstrated undoped ZnO nanorods inhibited 84.88 ± 0.37% α-glucosidase activity while Ag-doped ZnO nanorods resulted in 91.19 ± 0.37% inhibition. α-Amylase breaks down the complex starch into simple glucose while α-glucosidase catalyzes the 1,4-α-glucopyranosidic bond to produce α-glucose.[81,82] Inhibition of these key enzymes by BNPs helps in controlling post-prandial glucose level, therefore acting as anti-diabetic agents.

Besides antidiabetic activity, anti-glycation activity is also a remarkable ability of NPs. Glycation is a process of generating glucose related products under oxidative stress called as advanced glycation end products (AGEs) which end up in disrupting cell membrane and eventually apoptosis. The damaging effects of AGEs are associated with age and diabetes related diseases.[83] Therefore, in this study the efficacy of green synthesized BNPs in inhibiting vesperlysine-like AGEs and pentosidine-like AGEs was evaluated as anti-aging and anti-inflammatory tools. Fig. 8B reports highest vesperlysine-like AGEs and pentosidine-like AGEs was inhibited by Au–Ag BNPs as 61.93 ± 1.10% and 37.30 ± 0.60%, respectively. Au–ZnO BNPs resulted in 51.6 ± 0.60% and 32.35 ± 0.49% while Ag–ZnO BNPs in 42.76 ± 1.66% and 19.77 ± 0.89% inhibition of vesperlysine-like AGEs and pentosidine-like AGEs, respectively. Previous reports also shed light on the anti-glycation activities of AgNPs, ZnONPs and Ag–ZnO BNPs.[26,40,84] Here we have observed that spherical shaped smaller sized Au–Ag BNPs were better anti-glycation agents as compared to hybrid BNPs. The probable explanation for better activities of Au–Ag BNPs is that enzyme–NPs interaction vary depending on their size and shape. It is reported that curved NPs surface provides more flexibility to the adsorbed enzyme as compared to the planar NPs surface.[85] Furthermore, smaller size means greater surface area of NPs. A loss of enzyme activity results due to conformational changes in the active site of enzyme when enzyme interacts with NPs surface.[86] However further research is required in this domain to explore the underlying mechanism of antidiabetic and AGEs inhibition by NPs.

3.3.4. Anti-cancerous activities of BNPs

3.3.4.1. Cell viability assay of HepG2 cells by MTT. MTT assay was performed to find out the % of viable HepG2 cells when treated with BNPs. Fig. 9A shows a substantial loss of cell viability by Au–Ag BNPs (31.7 ± 3.46%), Au–ZnO BNPs (38.37 ±

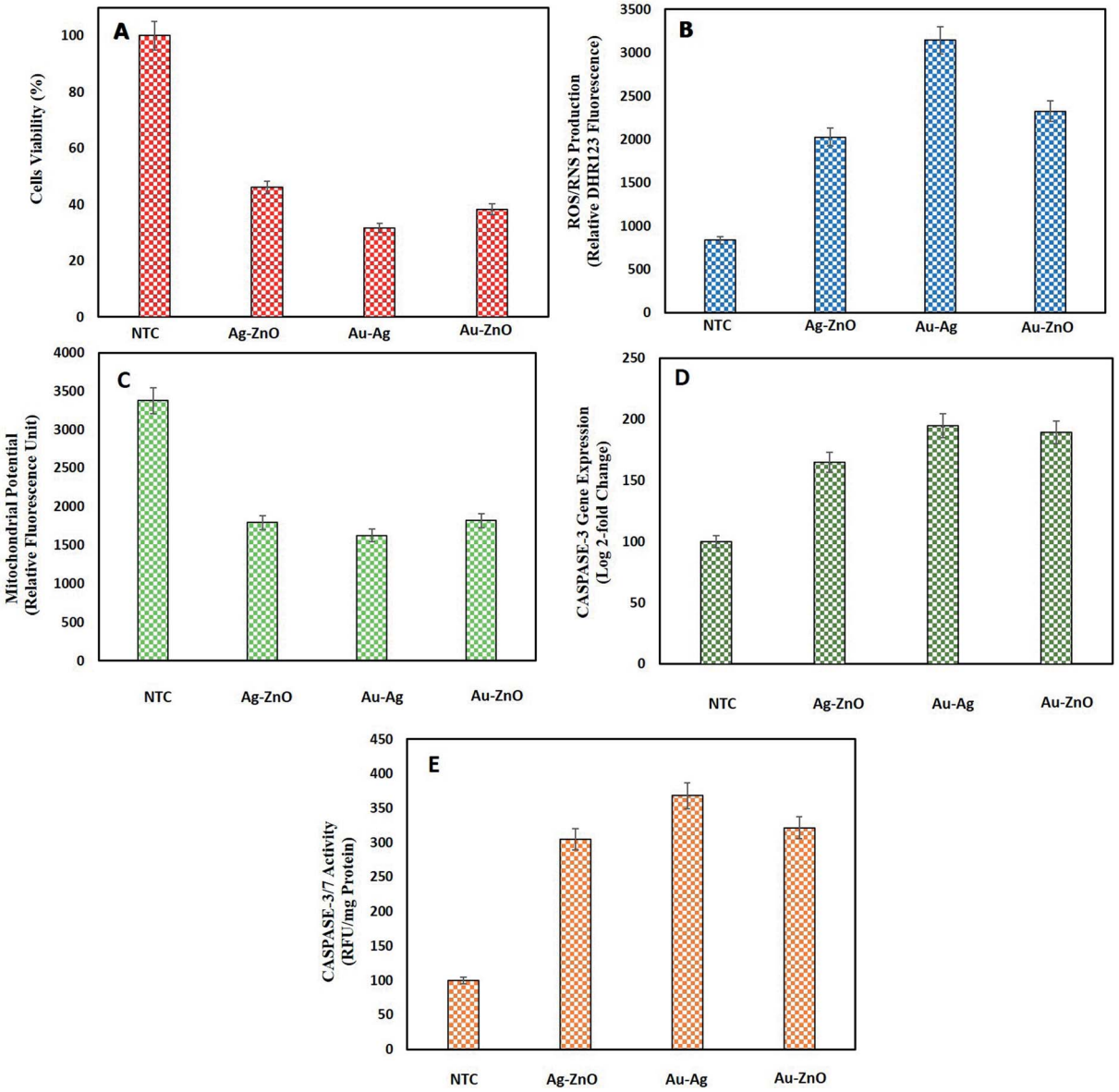

Fig. 9 BNPs activity against HepG2 cells (A) cell viability measurement (B) production of intracellular ROS/RNS (C) loss of mitochondrial membrane potential (D) caspase-3 gene expression (E) caspase-3/7 activity.

1.60%) and Ag–ZnO BNPs (46.02 ± 3.46%) as compared to NTC which were 100% viable. The large surface area of small sized Au–Ag BNPs were more cytotoxic towards HepG2 cells which was also confirmed from previous reports.[87] Previously bimetallic ZnO–Ag NPs synthesized *via* laser ablation method were found cytotoxic towards HeLa and HCT116 cancer cells at higher concentration as compared to their monometallic NPs.[88] Pandiyan *et al.*[16] reported exceptional anticancerous potential of Ag–Au/ZnO NPs against HeLa cell line which proves that bimetallic Ag and Au doping enhanced the anticancerous efficacy of ZnONPs.

3.3.4.2. Intracellular ROS/RNS production. Disproportional increase in intracellular ROS/RNS level can induce cancer cell cycle arrest and cell death.[89] Consequent escalation in intracellular ROS/RNS production in HepG2 cells in response to green synthesized BNPs is reported in Fig. 9B. In coherence with lowest cell viability, highest ROS/RNS were produced from Au–Ag BNPs 3143 ± 88.77 relative DHR123 fluorescence unit (RFU-DHR123). Furthermore, Au–ZnO BNPs resulted in 2325.3 ± 184.58 RFU-DHR123 and Ag–ZnO BNPs in 2025.28 ± 88.77 RFU-DHR123. The NTC produced normal level of intracellular ROS/RNS of 835 ± 80.17 RFU-DHR123. Sivamaruthi *et al.*[76] also verified ROS production in A549 lung cancer cells when exposed to bimetallic Ag–Pd NPs synthesized from *Terminalia chebula*. These findings shed light on the increase in intracellular stress by BNPs as a way to fight cancer.

3.3.4.3. Mitochondrial membrane potential. Injury to mitochondria is important in deciding the fate of cell especially apoptosis *i.e.* programmed cell death. Mitochondrial injury includes a loss of mitochondrial membrane permeability,

swelling of mitochondria, lysis of mitochondria and release of apoptotic proteins.[90] The loss of MMP in response to NPs is a key anti-cancerous strategy to kill cancer cells. In this study, notable loss of MMP in HepG2 cells was observed when incubated with green synthesized BNPs as shown in Fig. 9C. Au–Ag BNPs resulted in maximum loss of fluorescence 1626 ± 61.78 RFU representing the highest loss of MMP as compared to other synthesized BNPs. Ag–ZnO BNPs and Au–ZnO BNPs resulted in 1796.3 ± 61.09 RFU and 1820 ± 36.72 RFU, respectively as compared to NTC 3374.94 ± 105.31 RFU. 1947.40 ± 60.91 RFU loss of MMP was recorded when HepG2 cells were treated with biogenic ZnONPs while we report higher loss of MMP from bimetallic NPs.[13] These findings shows that bimetallic NPs are highly effective in disrupting MMP especially core–shell Au–Ag BNPs owing to their smaller size.

3.3.4.4. Caspase-3 gene expression and caspase-3/7 activity. Caspases are enzyme involved in the programmed cell death which is an outcome of the disruption of outer mitochondrial membrane pore and loss of MMP.[91] We also assessed the increase in caspase-3 gene expression as a result of BNPs treatment of HepG2 cells as a measure of anti-cancerous potential of green NPs. Fig. 9D shows induction of high level of caspase-3 gene expression by BNPs as compared to NTC (normalized to 100% (*i.e.*, 100 ± 1.81% in log 2 fold change basis)). Highest caspase-3 gene expression was induced by smaller sized spherical shaped Au–Ag BNPs 194.67 ± 4.51%. Au–ZnO BNPs resulted in 189.2 ± 8.50 and Ag–ZnO BNPs in 164.76 ± 11.06% caspase-3 gene expression. Here we can state that Au based bimetallic NPs show better cytotoxic properties due to their excellent optical features and biochemical consistency thereby enhancing the properties as bimetallic NPs. Katifelis *et al.*[92] reported that bimetallic Au–Ag alloy synthesized *via* chemical reduction activated caspase cascade in mice with tumor.

The consequent increase in caspase-3/7 activity was also observed correlating with caspase-3 gene expression. Au–Ag BNPs resulted in 368.23 ± 9.71, Au–ZnO BNPs 321.67 ± 15.72 and Ag–ZnO BNPs 304.67 ± 9.07 RFU per mg protein caspase-3/7 activity. The control showed 100 ± 6.61 RFU per mg protein caspase-3/7 activity. Baharara *et al.*[93] reported the induction of apoptosis through enhanced caspase-3/9 activity in HeLa cells by *Zataria multiflora* extract synthesized AuNPs. Sambale *et al.*[94] revealed high caspase 3/7 activity in A-549 cells cultivated with 10 ppm AgNPs indicating the cell death by apoptosis. These biocompatible BNPs synthesized from natural extract show anti-cancer activities which can be used as alternative to chemotherapeutic agents.

3.3.5. Proposed mechanism of anticancer activity of BNPs. The chemotherapeutic drugs available causes serious side effects to human health. Consequently, alternative, safe and effective anti-cancerous agents are required.[95] BNPs are one such nano-formulations known to exhibit cytotoxic effects against number of cancer cells.[96] The first step during NPs cytotoxicity against cancer cells is the internalization of NPs most probably *via* endocytosis pathway. Smaller sized NPs (approx. 10 nm) are said to coat plasma membrane prior to their incorporation whereas larger NPs (100 nm) are directly internalized without accumulating onto cell membrane.[92] The major endocytosis mechanisms for NPs uptake are phagocytosis, diffusion, pinocytosis and clathrin/caveolae-mediated endocytosis.[97] Factors such as NPs size, morphology, surface chemistry and incubation environment affect the uptake and internalization of NPs.[98]

Once internalized, NPs mediate cytotoxicity through several proposed mechanism. ROS and free radical generation is the key mechanism of NPs toxicity which induces oxidative stress.[99] In our study, we found enhanced level of ROS production in HepG2 cells when exposed to 200 μg mL^{-1} of green synthesized

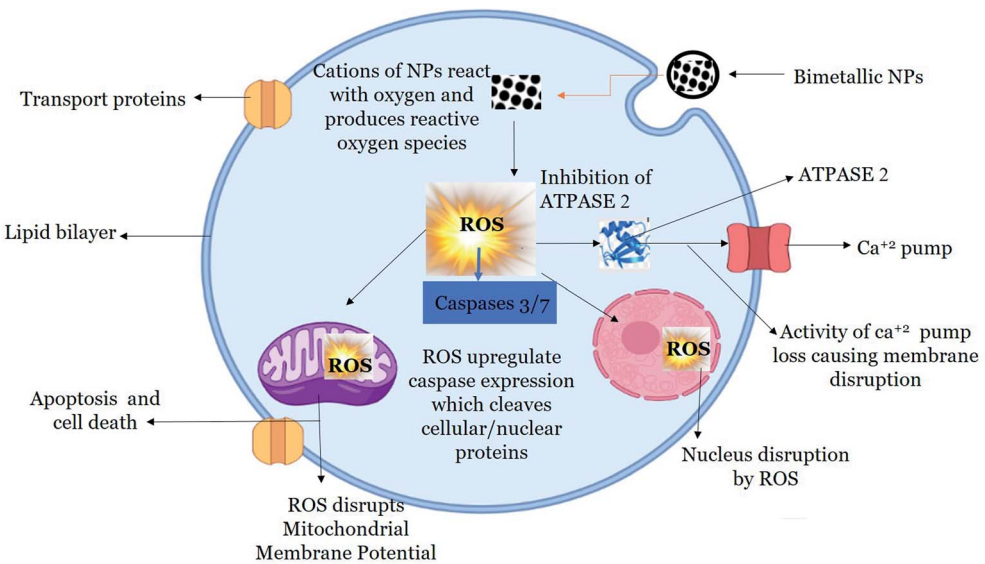

Fig. 10 Proposed anti-cancerous mechanism of green synthesized BNPs which are internalized into the cell *via* cell membrane, generates reactive oxygen species which activates caspases, disrupts MMP and eventually lead to the apoptosis of cancerous cells.

BNPs. The accumulation of ROS alters the health of cells by inhibiting Atpase-2 enzyme, which leads to the influx of extracellular Ca^{2+} ions.[100] Increase in intracellular Ca^{2+} ions particularly leads to mitochondrial dysfunction, DNA damage and fragmentation.[101] Mitochondria is the powerhouse as well as arsenal in cells, where cell death by apoptosis and non-apoptosis mechanism is triggered which results in disruption of electron transport, adenosine triphosphate production, oxidative phosphorylation, release of caspase protease and alteration in cellular reduction–oxidation potential.[102] The increase in intracellular ROS level opens mitochondrial transition pore which decreases MMP, initiates caspase cascade which eventually leads to cell death.[103] Caspases are intracellular proteases which are activated in a sequential manner and results in the formation of apoptotic bodies. Caspases 3 and 7 are effector caspases which executes apoptosis amongst other caspases.[104] The outcome of caspases include formation of apoptotic bodies, expression of ligands for phagocytic cell receptors and uptake of the apoptotic bodies by phagocytic cells. In our study, we found that BNPs effectively enhanced ROS level in HepG2 cells, which caused a loss of MMP. Furthermore, BNPs enhanced the activity of caspase-3 and caspase-7 which eventually led to cancer cells death evident from lower cell viability in HepG2 cells treated with BNPs as compared to NTCs. A possible mechanism is proposed in Fig. 10.

4 Conclusions

The plant based synthesis of BNPs provide a new scope for NPs synthesis being a simple and eco-friendly method. In our study, different BNPs including Au–ZnO, Au–Ag and Ag–ZnO were synthesized from *M. zapota* LE which possess rich content of bio-reducing and capping phytochemicals such as phenolic and flavonoid compounds. Characterization of NPs showed the size of Au–ZnO BNPs was 48.32 nm, Au–Ag BNPs 16.57 nm and Ag–ZnO BNPs 19.64 nm while a variety of shapes were formed. These green synthesized BNPs showed biocompatibility with human RBCs as well as brine shrimp larvae, therefore showing their biological and environmental safety. Furthermore, the BNPs particularly Au–Ag BNPs showed significant therapeutic activities including anti-cancerous against HepG2 cells, antibacterial, anti-diabetic and anti-glycations. We can conclude that the green synthesized BNPs have a potential to be used as future nano-medicine. Lastly future research should focus on developing green synthesis protocol which is scalable for mass production.

Ethical approval

The study was approved by the Bioethical committee of Kinnaird College for Women, Lahore, Pakistan.

Author contributions

Conceptualization, S. A and B. H. A.; methodology, K. N., S. A. and B. A.; validation, S. A., C. H., and B. H. A.; formal analysis, C. H., B. H. A. and S. A.; data curation, B. A., C. H., B. H. A. and S. A.; writing—original draft preparation, K. N., and S. A.; writing—review and editing, S. A., B. H. A. and C. H.; supervision, S. A. and C. H.; project administration, S. A.; funding acquisition, S. A. and C. H. All authors have read and agreed to the published version of the manuscript.

Conflicts of interest

Authors declare no conflict of interest.

References

1 G. Sharma, A. Kumar, S. Sharma, M. Naushad, R. Prakash Dwivedi, Z. A. Alothman and G. T. Mola, *J. King Saud Univ., Sci.*, 2019, **31**, 257–269.
2 R. M. C. R. Ramos and M. D. Regulacio, *ACS Omega*, 2021, **6**, 7212–7228.
3 A. Behera, B. Mittu, S. Padhi, N. Patra and J. Singh, in *Multifunctional Hybrid Nanomaterials for Sustainable Agri-Food and Ecosystems*, ed. K. A. Abd-Elsalam, Elsevier, 2020, pp. 639–682, DOI: 10.1016/B978-0-12-821354-4.00025-X.
4 A. Tulloch, A. Goldson-Barnaby, D. Bailey and S. Gupte, *Int. J. Fruit Sci.*, 2020, **20**, S1–S7.
5 A. L. Padilla-Cruz, J. A. Garza-Cervantes, X. G. Vasto-Anzaldo, G. García-Rivas, A. León-Buitimea and J. R. Morones-Ramírez, *Sci. Rep.*, 2021, **11**, 5351.
6 Y. Cao, H. A. Dhahad, M. A. El-Shorbagy, H. Q. Alijani, M. Zakeri, A. Heydari, E. Bahonar, M. Slouf, M. Khatami, M. Naderifar, S. Iravani, S. Khatami and F. F. Dehkordi, *Sci. Rep.*, 2021, **11**, 23479.
7 S. Gupta, H. Hemlata and K. Tejavath, *Beilstein Arch.*, 2020, **1**, 95.
8 K. Sathya, R. Saravanathamizhan and G. Baskar, *Mol. Biol. Rep.*, 2018, **45**, 1397–1404.
9 M.-T. Tsai, Y.-S. Sun, M. Keerthi, A. K. Panda, U. Dhawan, Y.-H. Chang, C.-F. Lai, M. Hsiao, H.-Y. Wang and R.-J. Chung, *Nanomaterials*, 2022, **12**, 61.
10 J. Ashraf, M. Ansari, S. Fatma, S. Abdullah, J. Iqbal, A. Madkhali, H. Hamali, S. Ahmad, A. Jerah, V. Echeverria, G. Barreto and G. Ashraf, *Mol. Neurobiol.*, 2018, **55**, 7438–7452.
11 F. Mohammadi Arvanag, A. Bayrami, A. Habibi-Yangjeh and S. Rahim Pouran, *Mater. Sci. Eng., C*, 2019, **97**, 397–405.
12 M. Bhardwaj, P. Yadav, S. Dalal and S. K. Kataria, *Biomed. Pharmacother.*, 2020, **127**, 110198.
13 A. K. Khan, S. Renouard, S. Drouet, J.-P. Blondeau, I. Anjum, C. Hano, B. H. Abbasi and S. Anjum, *Pharmaceutics*, 2021, **13**, 1977.
14 S. Anjum, B. H. Abbasi and C. Hano, *Plant Cell, Tissue Organ Cult.*, 2017, **129**, 73–87.
15 E. E. Elemike, D. C. Onwudiwe, O. E. Fayemi and T. L. Botha, *Appl. Phys. A: Mater. Sci. Process.*, 2019, **125**, 1–12.
16 N. Pandiyan, B. Murugesan, M. Arumugam, J. Sonamuthu, S. Samayanan and S. Mahalingam, *J. Photochem. Photobiol., B*, 2019, **198**, 111559.

17 Sumbal, A. Nadeem, S. Naz, J. S. Ali, A. Mannan and M. Zia, *Biotechnol. Rep.*, 2019, **22**, e00338.
18 D. Tungmunnithum, S. Renouard, S. Drouet, J.-P. Blondeau and C. Hano, *Plants*, 2020, **9**, 921.
19 S. Faisal, H. Jan, S. A. Shah, S. Shah, A. Khan, M. T. Akbar, M. Rizwan, F. Jan, Wajidullah and N. Akhtar, *ACS Omega*, 2021, **6**, 9709–9722.
20 S. Fakhari, M. Jamzad and H. Kabiri Fard, *Green Chem. Lett. Rev.*, 2019, **12**, 19–24.
21 M. F. Sohail, M. Rehman, S. Z. Hussain, Z.-E. Huma, G. Shahnaz, O. S. Qureshi, Q. Khalid, S. Mirza, I. Hussain and T. J. Webster, *J. Drug Delivery Sci. Technol.*, 2020, **59**, 101911.
22 B. H. Abbasi, S. Anjum and C. Hano, *RSC Adv.*, 2017, **7**, 15931–15943.
23 M. Ahmed, H. Fatima, M. Qasim and B. Gul, *BMC Complementary Altern. Med.*, 2017, **17**, 1–16.
24 A. T. Khalil, M. Ovais, I. Ullah, M. Ali, Z. K. Shinwari, S. Khamlich and M. Maaza, *Nanomedicine*, 2017, **12**, 1767–1789.
25 C. Hano, S. Renouard, R. Molinié, C. Corbin, E. Barakzoy, J. Doussot, F. Lamblin and E. Lainé, *Bioorg. Med. Chem. Lett.*, 2013, **23**, 3007–3012.
26 M. Shah, S. Nawaz, H. Jan, N. Uddin, A. Ali, S. Anjum, N. Giglioli-Guivarc'h, C. Hano and B. H. Abbasi, *Mater. Sci. Eng., C*, 2020, **112**, 110889.
27 B. H. Abbasi, M. Shah, S. S. Hashmi, M. Nazir, S. Naz, W. Ahmad, I. U. Khan and C. Hano, *Nanomaterials*, 2019, **9**, 1171.
28 M. Nazir, D. Tungmunnithum, S. Bose, S. Drouet, L. Garros, N. Giglioli-Guivarc'h, B. H. Abbasi and C. Hano, *J. Agric. Food Chem.*, 2019, **67**, 1847–1859.
29 N. Babbar, H. S. Oberoi, S. K. Sandhu and V. K. Bhargav, *J. Food Sci. Technol.*, 2014, **51**, 2568–2575.
30 L. H. Yao, Y.-M. Jiang, J. Shi, F. Tomas-Barberan, N. Datta, R. Singanusong and S. Chen, *Plant Foods Hum. Nutr.*, 2004, **59**, 113–122.
31 S. Islam, M. B. Alam, H.-J. Ann, J.-H. Park, S.-H. Lee and S. Kim, *Int. J. Mol. Sci.*, 2021, **22**, 132.
32 M. Kaneria and S. Chanda, *Asian Pac. J. Trop. Biomed.*, 2012, **2**, S1526–S1533.
33 S. Bawazeer, A. Rauf, S. U. A. Shah, A. M. Shawky, Y. S. Al-Awthan, O. S. Bahattab, G. Uddin, J. Sabir and M. A. El-Esawi, *Green Process. Synth.*, 2021, **10**, 85–94.
34 P. Molyneux, *Songklanakarin J. Sci. Technol.*, 2004, **26**, 211–219.
35 M. Khan, S. K. Behera, P. Paul, B. Das, M. Suar, R. Jayabalan, D. Fawcett, G. E. J. Poinern, S. K. Tripathy and A. Mishra, *Med. Microbiol. Immunol.*, 2019, **208**, 609–629.
36 Y. Weng, J. Li, X. Ding, B. Wang, S. Dai, Y. Zhou, R. Pang, Y. Zhao, H. Xu and B. Tian, *Int. J. Nanomed.*, 2020, **15**, 1823.
37 K. Gopinath, S. Kumaraguru, K. Bhakyaraj, S. Mohan, K. S. Venkatesh, M. Esakkirajan, P. Kaleeswarran, N. S. Alharbi, S. Kadaikunnan, M. Govindarajan, G. Benelli and A. Arumugam, *Microb. Pathog.*, 2016, **101**, 1–11.
38 D. Alti, M. Veeramohan Rao, D. N. Rao, R. Maurya and S. K. Kalangi, *ACS Omega*, 2020, **5**, 16238–16245.
39 Z. Zaheer and S. M. Albukhari, *Arab. J. Chem.*, 2020, **13**, 7921–7938.
40 S. Anjum, A. K. Khan, A. Qamar, N. Fatima, S. Drouet, S. Renouard, J. P. Blondeau, B. H. Abbasi and C. Hano, *Int. J. Mol. Sci.*, 2021, **22**, 11294.
41 T. Petit and L. Puskar, *Diamond Relat. Mater.*, 2018, **89**, 52–66.
42 S. Anjum and B. H. Abbasi, *Int. J. Nanomed.*, 2016, **11**, 715.
43 R. Geetha, T. Ashokkumar, S. Tamilselvan, K. Govindaraju, M. Sadiq and G. Singaravelu, *Cancer Nanotechnol.*, 2013, **4**, 91–98.
44 M. Roni, K. Murugan, C. Panneerselvam, J. Subramaniam and J.-S. Hwang, *Parasitol. Res.*, 2013, **112**, 981–990.
45 S. Some, O. Bulut, K. Biswas, A. Kumar, A. Roy, I. K. Sen, A. Mandal, O. L. Franco, İ. A. İnce and K. Neog, *Sci. Rep.*, 2019, **9**, 1–13.
46 S. Vennila and S. S. Jesurani, *Int. J. ChemTech Res.*, 2017, **10**, 271–275.
47 P. Kuppusamy, S. Ilavenil, S. Srigopalram, D. H. Kim, N. Govindan, G. P. Maniam, M. M. Yusoff and K. C. Choi, *J. Inorg. Organomet. Polym. Mater.*, 2017, **27**, 562–568.
48 B. Kim, W. C. Song, S. Y. Park and G. Park, *Catalysts*, 2021, **11**, 347.
49 R. Javed, M. Zia, S. Naz, S. O. Aisida, N. u. Ain and Q. Ao, *J. Nanobiotechnol.*, 2020, **18**, 172.
50 A. M. Mostafa and E. A. Mwafy, *J. Mater. Res. Technol.*, 2020, **9**, 3241–3248.
51 Y. Sun, Y. Sun, T. Zhang, G. Chen, F. Zhang, D. Liu, W. Cai, Y. Li, X. Yang and C. Li, *Nanoscale*, 2016, **8**, 10774–10782.
52 I. S. Saputra, D. O. B. Apriandanu, Y. Yulizar, E. Maryanti, Y. N. Permana, S. Suhartati and Sudirman, *Opt. Mater.*, 2021, **121**, 111628.
53 E. Csapó, A. Oszkó, E. Varga, Á. Juhász, N. Buzás, L. Kőrösi, A. Majzik and I. Dékány, *Colloids Surf., A*, 2012, **415**, 281–287.
54 S. Ganaie, T. Abbasi and S. Abbasi, *J. Exp. Nanosci.*, 2016, **11**, 395–417.
55 R. K. Sali, M. S. Pujar, S. Patil and A. H. Sidarai, *Adv. Mater. Lett.*, 2021, **12**, 1–7.
56 S. Slathia, T. Gupta and R. P. Chauhan, *Phys. B*, 2021, **621**, 413287.
57 F. Pragati, S. Gangopadhyay and S. Pande, *RSC Adv.*, 2014, **4**, 294962.
58 R. Biswas, B. Banerjee, M. Saha, I. Ahmed, S. Mete, R. A. Patil, Y.-R. Ma and K. K. Haldar, *J. Phys. Chem. C*, 2021, **125**, 6619–6631.
59 M. K. Choudhary, J. Kataria and S. Sharma, *ACS Appl. Nano Mater.*, 2018, **1**, 1870–1878.
60 M. Meena Kumari, J. Jacob and D. Philip, *Spectrochim. Acta, Part A*, 2015, **137**, 185–192.
61 N. Berahim, W. J. Basirun, B. F. Leo and M. R. Johan, *Catalysts*, 2018, **8**, 412.
62 S. Velpula, S. R. Beedu and K. Rupula, *Int. J. Biol. Macromol.*, 2021, **190**, 159–169.

63 M. Zare, K. Namratha, S. Alghamdi, Y. H. E. Mohammad, A. Hezam, M. Zare, Q. A. Drmosh, K. Byrappa, B. N. Chandrashekar, S. Ramakrishna and X. Zhang, *Sci. Rep.*, 2019, **9**, 8303.
64 S. Hameed, A. T. Khalil, M. Ali, M. Numan, S. Khamlich, Z. K. Shinwari and M. Maaza, *Nanomedicine*, 2019, **14**, 655–673.
65 P. M. Carvalho, M. R. Felício, N. C. Santos, S. Gonçalves and M. M. Domingues, *Front. Chem.*, 2018, **6**, 237.
66 M. I. Khan, S. K. Behera, P. Paul, B. Das, M. Suar, R. Jayabalan, D. Fawcett, G. E. J. Poinern, S. K. Tripathy and A. Mishra, *Med. Microbiol. Immunol.*, 2019, **208**, 609–629.
67 X. Jiang, X. Fan, W. Xu, R. Zhang and G. Wu, *ACS Biomater. Sci. Eng.*, 2019, **6**, 680–689.
68 Z. Noohpisheh, H. Amiri, S. Farhadi and A. Mohammadi-gholami, *Spectrochim. Acta, Part A*, 2020, **240**, 118595.
69 T. Mazhar, V. Shrivastava and R. S. Tomar, *J. Pharm. Sci. Res.*, 2017, **9**, 102.
70 K. Bankura, D. Maity, M. M. R. Mollick, D. Mondal, B. Bhowmick, I. Roy, T. Midya, J. Sarkar, D. Rana and K. Acharya, *Carbohydr. Polym.*, 2014, **107**, 151–157.
71 G. R. S. Andrade, C. C. Nascimento, Z. M. Lima, E. Teixeira-Neto, L. P. Costa and I. F. Gimenez, *Appl. Surf. Sci.*, 2017, **399**, 573–582.
72 A. Alshareef, K. Laird and R. B. M. Cross, *Appl. Surf. Sci.*, 2017, **424**, 310–315.
73 S. Hnamte, K. Kaviyarasu and B. Siddhardha, in *Model Organisms to Study Biological Activities and Toxicity of Nanoparticles*, Springer, 2020, pp. 401–415.
74 S. Krishnan Sundarrajan and L. Pottail, *Appl. Nanosci.*, 2021, **11**, 971–981.
75 C. M. Ramírez-Acosta, J. Cifuentes, J. C. Cruz and L. H. Reyes, *Nanomaterials*, 2020, **10**, 1857.
76 B. S. Sivamaruthi, V. S. Ramkumar, G. Archunan, C. Chaiyasut and N. Suganthy, *J. Drug Delivery Sci. Technol.*, 2019, **51**, 139–151.
77 M. Zare, K. Namratha, M. Thakur and K. Byrappa, *Mater. Res. Bull.*, 2019, **109**, 49–59.
78 U. Etxeberria, A. L. de la Garza, J. Campión, J. A. Martínez and F. I. Milagro, *Expert Opin. Ther. Targets*, 2012, **16**, 269–297.
79 V. Malapermal, J. N. Mbatha, R. M. Gengan and K. Anand, *Adv. Mater. Lett.*, 2015, **6**, 1050–1057.
80 P. Robkhob, S. Ghosh, J. Bellare, D. Jamdade, I. M. Tang and S. Thongmee, *J. Trace Elem. Med. Biol.*, 2020, **58**, 126448.
81 M. Kazmi, S. Zaib, A. Ibrar, S. T. Amjad, Z. Shafique, S. Mehsud, A. Saeed, J. Iqbal and I. Khan, *Bioorg. Chem.*, 2018, **77**, 190–202.
82 S. Poovitha and M. Parani, *BMC Complementary Altern. Med.*, 2016, **16**, 185.
83 P. Gkogkolou and M. Böhm, *Derm.-Endocrinol.*, 2012, **4**, 259–270.
84 J. M. Ashraf, M. A. Ansari, S. Fatma, S. Abdullah, J. Iqbal, A. Madkhali, A. H. Hamali, S. Ahmad, A. Jerah and V. Echeverria, *Mol. Neurobiol.*, 2018, **55**, 7438–7452.
85 A. Verma and F. Stellacci, *Small*, 2010, **6**, 12–21.
86 S. R. Saptarshi, A. Duschl and A. L. Lopata, *J. Nanobiotechnol.*, 2013, **11**, 26.
87 D. Sahu, G. Kannan, M. Tailang and R. Vijayaraghavan, *J. Nanosci.*, 2016, **2016**, 1–9.
88 K. A. Elsayed, M. Alomari, Q. A. Drmosh, M. Alheshibri, A. Al Baroot, T. S. Kayed, A. A. Manda and A. L. Al-Alotaibi, *Alexandria Eng. J.*, 2022, **61**, 1449–1457.
89 G.-Y. Liou and P. Storz, *Free Radical Res.*, 2010, **44**, 479–496.
90 S. Hussain, in *Nanotoxicity*, Springer, 2019, pp. 123–131.
91 Q. Tang, H. Xia, W. Liang, X. Huo and X. Wei, *J. Photochem. Photobiol., B*, 2020, **202**, 111698.
92 H. Katifelis, I. Mukha, P. Bouziotis, N. Vityuk, C. Tsoukalas, A. C. Lazaris, A. Lyberopoulou, G. E. Theodoropoulos, E. P. Efstathopoulos and M. Gazouli, *Int. J. Nanomed.*, 2020, **15**, 6019.
93 J. Baharara, T. Ramezani, A. Divsalar, M. Mousavi and A. Seyedarabi, *Avicenna J. Med. Biotechnol.*, 2016, **8**, 75.
94 F. Sambale, S. Wagner, F. Stahl, R. Khaydarov, T. Scheper and D. Bahnemann, *J. Nanomater.*, 2015, **16**(1), 1–6.
95 L. Le Marchand, *Biomed. Pharmacother.*, 2002, **56**, 296–301.
96 H. Chen, L. Luo, S. Fan, Y. Xiong, Y. Ling and S. Peng, *J. Pharm. Pharmacol.*, 2021, **73**, 221–232.
97 N. Oh and J.-H. Park, *Int. J. Nanomed.*, 2014, **9**, 51.
98 F. Gulbagça, A. Aygun, E. E. Altuner, M. Bekmezci, T. Gur, F. Sen, H. Karimi-Maleh, N. Zare, F. Karimi and Y. Vasseghian, *Chem. Eng. Res. Des.*, 2022, **180**, 254–264.
99 K. A. Elsayed, M. Alomari, Q. Drmosh, M. Alheshibri, A. Al Baroot, T. Kayed, A. A. Manda and A. L. Al-Alotaibi, *Alexandria Eng. J.*, 2022, **61**, 1449–1457.
100 S. Zhu, L. Gong, Y. Li, H. Xu, Z. Gu and Y. Zhao, *Adv. Sci.*, 2019, **6**, 1802289.
101 K.-N. Yu, T.-J. Yoon, A. Minai-Tehrani, J.-E. Kim, S. J. Park, M. S. Jeong, S.-W. Ha, J.-K. Lee, J. S. Kim and M.-H. Cho, *Toxicol. in Vitro*, 2013, **27**, 1187–1195.
102 B. Javed, M. Ikram, F. Farooq, T. Sultana, Z.-u.-R. Mashwani and N. I. Raja, *Appl. Microbiol. Biotechnol.*, 2021, **105**, 2261–2275.
103 G. Chen, S.-Y. Li, H. T. Malik, Y.-G. Ma, H. Xu and L.-K. Sun, *Biotechnol. Lett.*, 2016, **38**, 1269–1276.
104 F. Mobaraki, M. Momeni, M. E. T. Yazdi, Z. Meshkat, M. S. Toosi and S. M. Hosseini, *Process Biochem.*, 2021, **111**, 167–177.